Multi-Feature Representation Based COVID-19 Risk Stage Evaluation With Transfer Learning

Xiangjie Kong, *Senior Member, IEEE*, Ning Li, Chenwei Zhang, Guojiang Shen, Zhaolong Ning, *Senior Member, IEEE*, and Tie Qiu, *Senior Member, IEEE*

***Abstract*—Accurate real-time COVID-19 confirmed case prediction and risk stage evaluation are of great significance for government decision-making. However, the complexity of the epidemic spread and the lack of data in countries where COVID-19 has recently emerged are still an important challenge for researchers. In this paper, we propose a multi-feature representation based COVID-19 risk stage evaluation model with transfer learning (COV2RS) to solve these issues. Specifically, by analyzing COVID-19 spatio-temporal characteristics, we build a spatial epidemic spread network and obtain multi-feature representation using a hierarchical spatio-temporal framework. From this, we obtain the COVID-19 confirmed case prediction results by aggregating representations. Finally, with transfer learning, we utilize COVID-19 confirmed data from other countries to evaluate the risk stage. Experiments based on real-world COVID-19 datasets demonstrate that our prediction results outperform the state-of-the-art baselines and can evaluate the COVID-19 risk stage well.**

***Index Terms*—COVID-19 risk stage evaluation, multi-feature representation, epidemic spread, spatio-temporal dependence, transfer learning.**

I. Introduction

With the increasing severity of the international COVID-19 epidemic, the forecast of confirmed cases and the evaluation of risk stage are critical for a country's future arrangements, such as whether cities should be closed, travel restrictions implemented, or businesses shuttered to prevent cluster infection cases. On the one hand, blindly stopping production will have an adverse impact on the economy and development of the country [1]; on the other hand, blindly resuming production for short-term economic benefits will increase the risk of COVID-19 epidemic clustering in the longer term when a country is still in a high risk stage. This would lead to the epidemic developing in a more serious direction, exacting a huge cost, both socioeconomically and lives. At the same time, prediction of future COVID-19 confirmed cases [2] and assessment of the current risk stage can guide the arrangements of various social resources, such as the preparation of medical supplies and medical personnel, as well as medical companies' production levels. When future demand surges, additional labor can be recruited to increase production. When future demand decreases, overtime should be controlled to prevent excessive production of medical supplies.

However, the exploration of the implicit relationship of multi-source heterogeneous COVID-19 data, the analysis of COVID-19 data's spatio-temporal complexity, and the lack of COVID-19 data all bring huge challenges:

- *Multi-Source Heterogeneous Data*: Social networks are generally considered to be the most real-time networks. The data generated by these networks is more real-time and spread faster with data from other sources. In observing the changes in COVID-19 confirmed cases and COVID-19 search interest on online networks [3], [4], as shown in Fig. 1, we clearly found that the latter successfully predicts trend in the former. Zheng *et al.* [5] illustrated that language information processing of related news can help improve the accuracy of the COVID-19 prediction model. There are many sources of COVID-19-related data, such as environmental temperature [6], degree of social isolation, latitude and longitude, population base, population density, and age distribution. And multiple different sources of data lead to COVID-19 data heterogeneity. In the data preparation part, we solved the heterogeneous problem of data from different sources. Studies [6]–[8] have shown that these features have an important impact on the spread of the COVID-19 epidemic. Bannister-Tyrrell *et al.* [6] analyzed the impact of temperature on the spread of the epidemic. Shokouhi *et al.* [7] analyzed the impact of latitude, longitude, and humidity on the spread of the epidemic. Buckner *et al.* [8] analyzed the impact of age distribution on the spread of the epidemic. Elucidating the implicit relationships of these features, however, will be a challenge.

Manuscript received April 17, 2021; revised December 15, 2021; accepted January 9, 2022. Date of publication January 13, 2022; date of current version May 23, 2022. This work was supported in part by the National Natural Science Foundation of China under Grants 62072409 and 62073295, in part by Zhejiang Provincial Natural Science Foundation under Grant LR21F020003, in part by Dalian Young Science and Technology Star under Grant 2020RQ002, and in part by the Fundamental Research Funds for the Provincial Universities of Zhejiang under Grant RF-B2020001. Recommended for acceptance by Dr. Caterina Scoglio. *(Corresponding author: Guojiang Shen.)*

Xiangjie Kong, Ning Li, and Guojiang Shen are with the College of Computer Science and Technology, Zhejiang University of Technology, Hangzhou 310023, China (e-mail: xjkong@ieee.org; ningli68@outlook.com; gjshen1975@zjut.edu.cn).

Chenwei Zhang is with the School of Faculty of Education, University of Hong Kong, Hong Kong (e-mail: chwzhang@hku.hk).

Zhaolong Ning is with the School of Software, Dalian University of Technology, Dalian 116024, China (e-mail: zhaolongning@dlut.edu.cn).

Tie Qiu is with the School of Computer Science and Technology, College of Intelligence and Computing, Tianjin University, Tianjin 300350, China (e-mail: qiutie@ieee.org).

Digital Object Identifier 10.1109/TNSE.2022.3142316

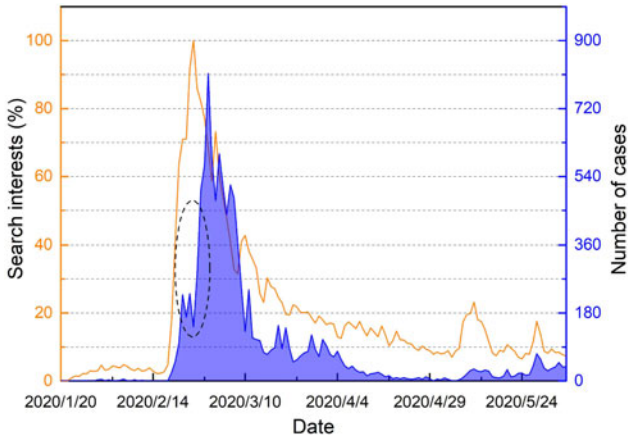

Fig. 1. The yellow line represents South Korea's COVID-19 search interests (including corona, coronavirus, COVID-19, covid, etc.) on Naver (an influential South Korean search engine). It shows that the search interests have a predictive effect on the trend of COVID-19 confirmed cases. The black dotted oval shows that the COVID-19 confirmed cases have tendency change within consecutive days.

- *Spatio-Temporal Complexity*: The development of the COVID-19 epidemic has certain observed spatial characteristics. As shown in Fig. 2(a), it is generally spread from the high-risk areas of the epidemic to the surrounding areas. Confirmed case counts change dynamically over time and are often related to the trend. As shown in Fig. 1, the number of confirmed cases is affected by the case count of the previous day or even earlier.
- *Lack of Data*: We do not have confirmed COVID-19 data for the complete cycle in countries where COVID-19 has just broken out, and it is very difficult to directly evaluate the current COVID-19 risk stage. Data transfer from countries worldwide that have already experienced COVID-19 is a key problem.

To solve the above problems, we propose COV2RS. Our main contributions are threefold:

- A hierarchical spatio-temporal representation framework is designed to effectively analyze the COVID-19's spatio-temporal dependence for COVID-19 prediction by analyzing outbreaks' spatio-temporal characteristics.
- We propose data transfer methods to solve the lack of data for COVID-19 evaluation by mapping the source domain to the target domain and transferring data between countries.
- We evaluated our model on a real-world COVID-19 confirmed case dataset. It is found that our multi-feature-based model for COVID-19 confirmed case prediction exhibits better performance than other state-of-the-art methods. The model's risk stage evaluation attains high accuracy.

The rest of the paper is organized as follows. We briefly review related work in Section II. In Section III, we provide a detailed description of the COVID-19 multi-features, COVID-19 risk stage and problem definition. Section IV introduces the details of our method. Section V illustrates the datasets and reports the model's experimental performance. And Section VI concludes the paper.

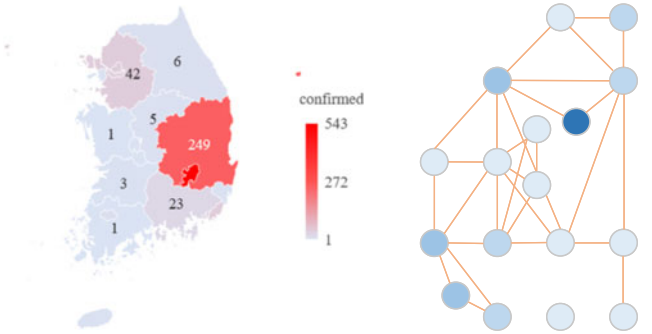

Fig. 2. (a) Spatial distribution of cumulative confirmed COVID-19 cases in South Korea on February 25. (b) Provincial network constructed based on provincial adjacency.

II. Releted Work

In related research to the COVID-19 epidemic, we have found that multi-feature data, the temporal and spatial characteristics of the epidemic, and the transfer data played a key role. We review the related paper on epidemic spread, spatio-temporal representation methods, and transfer learning. General models use graph and SIR model to model the COVID-19 diffusion. For example, Schlosser *et al.* [10] analyzed mobility networks from mobile phones of 43.6 million individuals in Germany and modeled mobility to the SIR model to obtain the prediction results. La Gatta *et al.* [11] modeled mobility data through a graph series in order to infer the parameters of SIR and SIRD models. Our model does not use the SIR model, instead directly uses graph to model COVID-19 diffusion. This is a data-driven method. This method can use more data than traditional methods and uses the powerful learning ability of neural networks to build a more efficient model, breaking through the inherent limitations of the SIR model.

A. Epidemic Spread

In recent years, with the development of Internet technology and wireless sensor technology [9], Internet search data, virus gene data, geographic information data and other multi-feature data have been used to analyze the spread of viruses [12]–[14]. Since multi-source data participates in epidemic spread modeling, the model can better dig out the law of epidemic spread. Internet search data in particular has been used in the modeling and analysis of common viruses such as influenza [16], [17]; compared with traditional epidemiological data, Internet search data exhibits small-time delays, a strong real-time character, wide survey scope, and high stability. In 2009, Google proposed the Google flu system for the first time, which used Internet search data to predict flu trends [16]. Subsequent researchers continued to improve statistical methods and have obtained higher-precision real-time prediction results [17]. At the same time, the role of viral genetic data in infectious disease modeling has gradually emerged since 2004 [18]. Researchers have analyzed genetic differences in viruses such as Ebola and HIV [12], [15] in different infected individuals to construct a virus phylogeny and

TABLE I
MAIN DISTINCTIONS AMONG DEEP LEARNING METHODS ON GRAPHS

Category	Type	Node Attributes/Labels	Main Function
Graph Neural Networks	Semi-supervised	Yes	Definitions of states for nodes or graphs
Graph Convolutional Networks	Semi-supervised	Yes	Graph convolution and readout operations
Graph Autoencoders	Unsupervised	Partial	Unsupervised node representation learning
Graph Reinforcement Learning	Semi-supervised	Yes	Graph-based actions and rewards
Graph adversarial methods	Semi-supervised	Yes	Graph adversarial trainings and attacks

inferred key information such as when the infection occurred. In addition, electronic medical record data and geographic information have also found wide use in infectious disease modeling [19]. At this stage of development, statistical methods can easily fuse diverse information and play an important role in research. Our model attempts to combine COVID-19 multi-feature data with neural networks and achieve higher-precision predictions through the powerful capabilities of machine learning.

B. Spatio-Temporal Representation

In recent years, due to the efficient representation of graph spatial structure data [20], graph structure models have become widespread. The graph models currently in use can largely be divided into graph neural networks (GNNs) and Graph Convolutional Networks (GCNs). GNNs combine graphs and recurrent neural networks; through multiple iterations of message transmission and node states update, each node captures the semantic relation and structural information between adjacent nodes. GCNs can be further divided into two types: spectral GCNs and spatial domain GCNs. Spectral GCNs transform the graph signals on the spectral domains of the graph, then apply spectral filters on these domains. Spatial GCNs use convolution operations to calculate a new feature vector of a node using the neighborhood information of each node. Shen *et al.* [21] used spatial GCNs to greatly enhance the commercial distribution discovery capabilities of the framework. Table I summarize the main graph representation models [22]. Different graph representation models have different application areas. In addition, recurrent neural networks (RNNs), including LSTM and GRU, can learn temporal representation well and achieve better prediction results [23] by using the self-circulation mechanism. In order to capture the spatio-temporal characteristic representation of the graph sequence, Seo *et al.* [24] first proposed a graph convolutional LSTM, which is an extension of GCNs and has a recurrent architecture. Several other recent studies [25], [26] further showed that learning discriminative spatio-temporal feature representation is the key to human behavior recognition. La Gatta *et al.* [11] modeled mobility data through a graph series whose spatial and temporal features are investigated by combining GCNs and LSTM in order to infer the parameters of SIR and SIRD models. Inspired by these papers, we propose a hierarchical spatio-temporal representation method.

C. Transfer Learning

In our research, there are major differences in confirmed case count between different countries. Thus, these data are considered to be in different categories. If COVID-19 data can be successfully transferred, the lack of data in the target domain can be avoided. According to survey [27], transfer learning methods can be divided into four groups: instance-based, feature-based, parameter-based, and relational-based. Instance-based transfer learning methods are mainly based on the instance weighting strategy. For example, Sugiyama *et al.* [28] proposed a method called Kullback-Leibler Importance Estimation Procedure (KLIEP) to estimate the weights. Dai *et al.* [29] proposed the TrAdaBoost framework to reduce the weights of instances that have a negative impact on the target learner. This latter framework is an extension of AdaBoost [30] to the transfer learning scenario. In TrAdaBoost, the labeled source domain instances and the labeled target domain instances are combined into a whole, i.e., a training set, which is used to train the weak classifier. Jiang and Zhai [31] proposed a general weighting framework to realize the instance weighting strategy in a heuristic way. Feature-based methods transform the original features to create a new feature representation [32]; they can be further divided into two subcategories, i.e., asymmetric transfer learning and symmetric feature-based transfer learning. Asymmetric methods transform the source features to match the target features; in contrast, symmetric methods try to find a common latent feature space, then convert both the source features and the target features into a new feature representation. Parameter-based transfer learning methods [33] transfer knowledge at the model/parameter level, and relational-based methods, which mainly focus on relational domain problems, transfer the logical relationships or rules learned in the source domain to the target domain. Inspired by prior work on instance-based, here we propose the methods to address the lack of data for COVID-19 risk stage evaluation.

III. PRELIMINARY

A. COVID-19 Multi-Features

The spread of the COVID-19 epidemic is often related to multiple features. Thus, in our research, we collected a wealth of demographic, geographic, and behavioral features relevant to the epidemic. These are described in Table V and fall into two major categories: province-level features and country-level features. All these features are used as inputs of our model to explore the trend of COVID-19 epidemic.

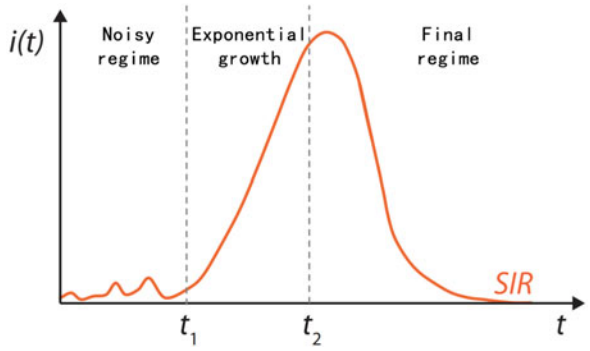

Fig. 3. When an epidemic erupts, typical profile of the density $i(t)$ of infected individuals versus time. In the first regime ($t < t_1$), the outbreak is subject to strong statistical fluctuations. In the second regime ($t_1 < t < t_2$), there is an exponential growth characterized. In the final regime ($t > t_2$), the density of infected individuals converges to zero, for SIR-like models [35]. We call the entire process a complete epidemic confirmed cycle. $i(t)$ represents all confirmed cases; number of cases in this paper represents daily confirmed cases.

B. COVID-19 Risk Stage

There is at present no uniform standard for evaluating a country's COVID-19 risk stage. Abdulsalam *et al.* [34] proposed a novel epidemic risk assessment method on the basis of the communication station's information. The existing evaluation standards are generally based on the number of COVID-19 confirmed cases. However, these quantity-based risk stage evaluation methods have many problems: one is that the future trend of the COVID-19 epidemic is not known, and the other is that the risk stage of the epidemic cannot be evaluated from the perspective of a complete COVID-19 confirmed case cycle. Fig. 3 is a complete epidemic confirmed cycle. Our evaluation standard is based on the complete COVID-19 confirmed case cycle. The specific evaluation standard is shown in Definition 3.

C. Problem Definition

Definition 1: Provincial Network G. We use the unweighted graph $G = (V; E)$ to describe the topological structure of the provincial network. We regard each province as a node, where V represents a series of province network nodes $V = \{v_1, v_2, v_3, \ldots, v_N\}$, N represents the number of nodes, and E represents a set of edges. The adjacency matrix A is used to represent the connection between provinces, $A \in R^{N\times N}$; it contains only elements of 0 (if there is no link between the two provinces) and 1 (if there is a link).

Definition 2: Feature Matrix $\mathrm{X}^{N\times P}$. We regard the COVID-19 features of each province as the attributes of the node in the network, expressed as $\mathrm{X} \in \mathrm{R}^{N\times P}$, where P represents the number of attributes and N represents the number of provinces. The node attributes are related to COVID-19 such as environmental temperature, degree of social isolation, latitude and longitude, population base, population density, age distribution, etc.

Definition 3: COVID-19 Risk Stage. We propose a new standard–recent to max (rtm)–to describe the COVID-19 status of the country.

TABLE II
COVID-19 RISK STAGE STANDARD

rtm range	COVID-19 risk stage
[0, 0.2)	Low(0)
[0.2, 0.5)	Medium(1)
[0.5,0.8)	High(2)
[0.8,+∞)	Severe(3)

$$rtm = \frac{rdc}{mdc} = \frac{(case_{i-1} + case_i + case_{i+1})/3}{(case_{max1} + case_{max2} + case_{max3})/3} \quad (1)$$

where rdc represents the average of COVID-19 confirmed cases over the previous three days. Including too few days results in oversensitivity to daily fluctuations; including too many days leads to poor differentiation of countries with high ratios in the early phase. Three days is reasonable and allows the model to keep up with the latest growth trend. mdc represents the average of the three days with the largest numbers of confirmed cases in the complete COVID-19 confirmed case cycle. In order to eliminate errors as much as possible, we choose three days. The higher the rtm, the more severe the epidemic, and the lower the rtm, the milder the epidemic. Table II presents the evaluation standard of COVID-19 risk stage. These rtm ranges for different risk stages correspond to the regime of the epidemic cycle in Fig. 3 (Noisy regime – Medium, Exponential – High and Severe, Final regime – low.). The rtm ranges are obtained by analyzing the epidemic confirmed data of each regime. After many attempts, this classification standard is the one most in line with our current research. Labeled graphs of a complete COVID-19 confirmed cycle is shown in Fig. 4. We can clearly see that the distribution of the labels fits the development of the cycle well. Table III lists symbols used in our experiment.

IV. METHODOLOGY

A. Overview

The architecture of the proposed COV2RS model is shown in Fig. 5. The model consists of three major parts: multi-feature hierarchical spatio-temporal representation, COVID-19 confirmed case prediction and COVID-19 risk stage evaluation. The first part is further divided into two layers: the provincial level and the country level. At the provincial level, we first use the n historical time series provincial P-dimensional COVID-19 features (geographical features, weather features, demographic features, etc.) as input, and the GCN is used to learn the topological structure of the province network to obtain spatial dependence. Then the obtained time series temporal features with spatial dependence are input into the LSTM cells to capture temporal dependence. Finally, we obtain the provincial-level COVID-19 multi-feature spatio-temporal fusion representation. At the country level, we first use the n historical time series countrywide COVID-19 features (Internet search interests and basic confirmed case count) as input, and the GRU is used to capture temporal dependence.

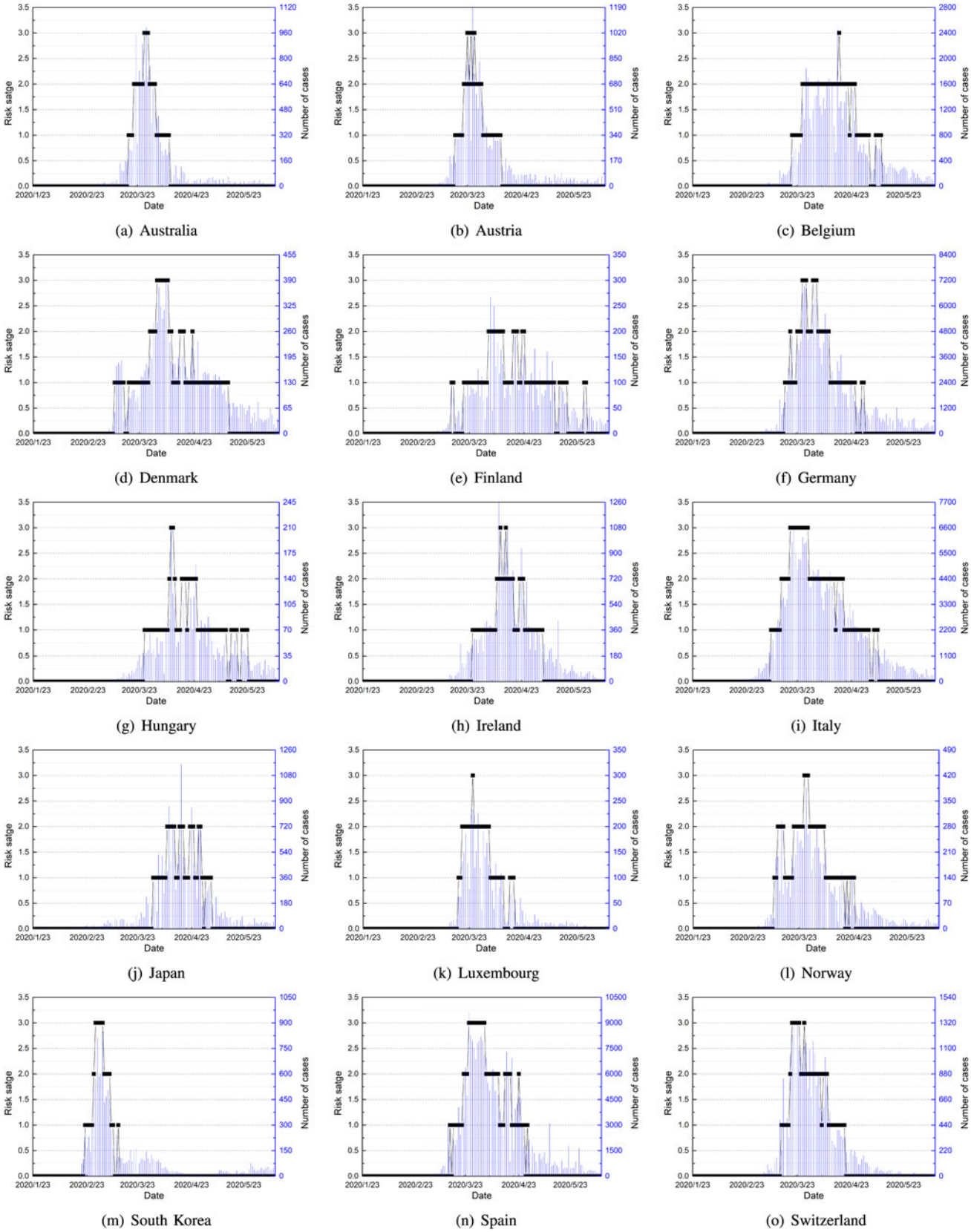

Fig. 4. All countries' COVID-19 risk stage distribution across the entire confirmed COVID-19 cycle.

TABLE III
DESCRIPTION OF NOTATIONS

Notation	Description
X^e	Decoder input
rtm	COVID-19 risk status
Ch_n	Trend characteristics of data
$Data_n$	Part of the source Data
$Tlabel$	Real COVID-19 risk stage
$Plabel$	COVID-19 risk stage evaluation results
N_n	Normalization method of data
P	Number of node/province attributes
Si	Similarity between $Tlabel$ and $Plabel$
$case_n$	Number of COVID-19 confirmed cases
rdc	Average of 3-day confirmed COVID-19 cases
N	Number of nodes/provinces in the provincial network
mdc	Average of the 3-day maximum COVID-19 confirmed cases

Then we obtain the country-level COVID-19 multi-feature temporal fusion representation. In the second part of the model (case prediction), two representation vectors input the fully connected layer to obtain the COVID-19 confirmed case prediction result. In part three (risk stage evaluation), the prediction result combines with four historical time series of COVID-19 confirmed cases as the decoder input to evaluate the current COVID-19 risk stage. To train decoders, we propose data transfer methods. These methods obtain the data of the target domain $Data_{target}$ from the global COVID-19 dataset $Data_{source}$.

B. Multi-Feature Hierarchical Spatio-Temporal Representation

Data Preparation. We select 24 provincial features and two country features, and each feature is normalized to [0, 1] according to the maximum value of the feature.

Provincial Multi-Feature Spatial-Temporal Representation. COVID-19 outbreaks always display regional clustering, so obtaining complex spatial dependence is a key point in predicting COVID-19 confirmed cases. A traditional convolutional neural network (CNN) can obtain local spatial characteristics, but it can only be used in Euclidean space, such as images, regular grids, etc. However, the area connection is complex, not a two-dimensional grid, which means that the CNN model cannot reflect the complex topology of the epidemic outbreak area and cannot accurately capture its spatial dependence. The GCN model has been successfully used in many applications, including document classification [36] and unsupervised learning [37]. Given the adjacency matrix A and the feature matrix X, the GCN model constructs a filter in the Fourier domain. The filter acts on the nodes of the graph, obtains the spatial characteristics between the nodes through the first-order neighborhood of the nodes, and then builds the GCN model by superimposing multiple convolutional layers, which can be expressed as:

$$X^{(l+1)} = \sigma\left(\tilde{D}^{-\frac{1}{2}}\tilde{A}\tilde{D}^{-\frac{1}{2}}X^{(l)}W^{(l)}\right) \tag{2}$$

where $\tilde{A} = A + I_N$ is the matrix with added self-connections, I_N is the identity matrix, $\tilde{D}$ is the degree matrix, $\tilde{D} = \sum_j \tilde{A}_{ij}$, $X^{(l)}$ is the input, $W^{(l)}$ represents the weight matrix and $\sigma(\cdot)$ represents the sigmoid function.

In our research, the spatio-temporal cell (STCell) construction at the provincial level is shown in Fig. 6. First, we use the two-layer GCN model to obtain its spatial characteristics.

$$f(X, A) = sigmoid\Big(\hat{A}\mathrm{ReLU}\Big(\hat{A}XW^{(0)}\Big)W^{(1)}\Big) \tag{3}$$

where $\hat{A} = \tilde{D}^{-\frac{1}{2}}\tilde{A}\tilde{D}^{-\frac{1}{2}}$ is a pre-processing step, $W^{(0)} \in R^{P\times H}$ represents the input-to-hidden weight matrix, and $W^{(1)} \in R^{H\times F}$ represents the hidden-to-output weight matrix. ReLU() is Rectified Linear Unit, and $f(X, A) \in R^{N\times F}$ represents the output after two layers of convolution. Here, multi-feature data X are input to the two-layer GCN to learn the spatial dependence of COVID-19 confirmed data. Then the output $f(X, A) \in R^{N\times F}$ is used as input for an LSTM cell to learn its temporal dependence.

$$\begin{aligned}
i_t &= \sigma(W_{xi} * f(X, A) + W_{hi} * H_{t-1} + b_i)\\
f_t &= \sigma\big(W_{xf} * f(X, A) + W_{hf} * H_{t-1} + b_f\big)\\
g_t &= \tanh\big(W_{xg} * f(X, A) + W_{hg} * H_{t-1} + b_g\big)\\
o_t &= \sigma(W_{xo} * f(X, A) + W_{ho} * H_{t-1} + b_o)\\
C_t &= f_t \odot C_{t-1} + i_t \odot g_t\\
H_t &= o_t \cdot \tanh(C_t)
\end{aligned} \tag{4}$$

where $\odot$ represents the Hadamard product. After the above series of calculations, the last H_t is used as the provincial level multi-feature representation.

Country Multi-feature Temporal Representation. At the country level, we combine the data of COVID-19 search interests $X_s \in R^{1\times 1}$ and daily confirmed cases $X_f \in R^{1\times 1}$ into $X_{sf} \in R^{1\times 2}$. This is then entered into the GRU. The trend of COVID-19 search interests, combined with the historical trend in confirmed cases, further grasp the future trend in confirmed cases.

$$\begin{aligned}
u_t &= \sigma\big(W_{xu} * X_{sf} + W_{hu} * h_{t-1} + b_u\big)\\
r_t &= \sigma\big(W_{xr} * X_{sf} + W_{hr} * h_{t-1} + b_r\big)\\
c_t &= \tanh\big(W_c\big[X_{sf}, (r_t * h_{t-1}) + b_c\big]\big)\\
h_t &= u_t * h_{t-1} + (1 - u_t) * c_t
\end{aligned} \tag{5}$$

where h_t is the country level multi-feature representation.

C. COVID-19 Confirmed Case Prediction

Hierarchical Aggregation Prediction: Next, we use a fully connected layer to aggregate the representation results and obtain the COVID-19 prediction result.

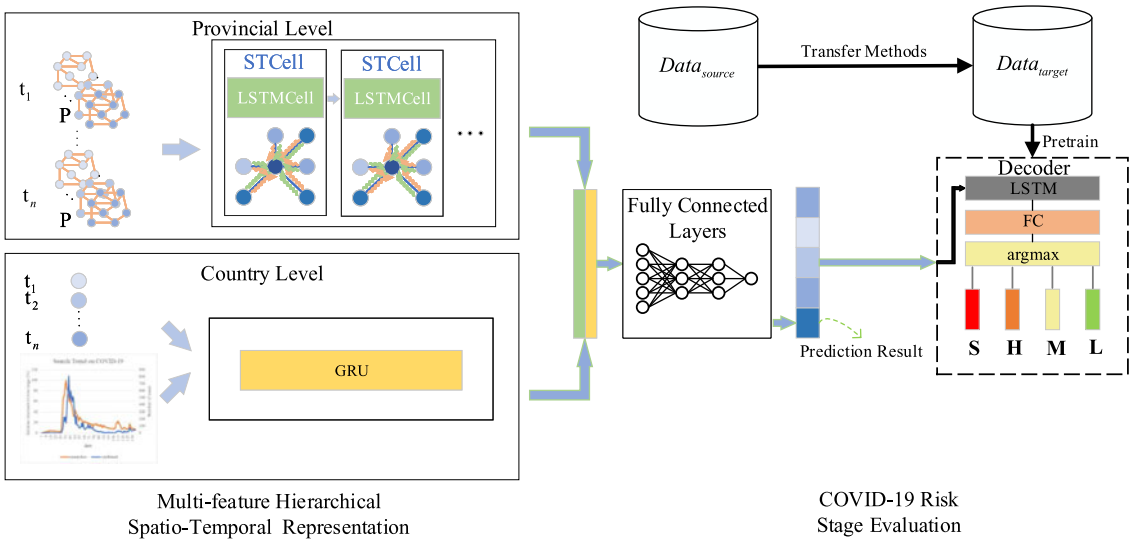

Fig. 5. The architecture of the proposed COV2RS model. Firstly, STCell (consisting of GCNs and LSTM cell) is used to capture provincial COVID-19 multi-feature spatio-temporal dependence and to obtain a provincial representation. GRU is used to capture country-level COVID-19 multi-feature temporal dependence and to obtain the country representation. Then, the representation vectors are used as input into the fully connected layer to obtain the corresponding COVID-19 confirmed case prediction result. Finally, we use data transfer methods to train the decoder. The input is the previous COVID-19 confirmed case prediction result along with 4 historical daily confirmed case counts. The decoder consists of a layer of LSTM, a fully connected layer and the argmax function, and the decoder is used to evaluate the COVID-19 risk stage.

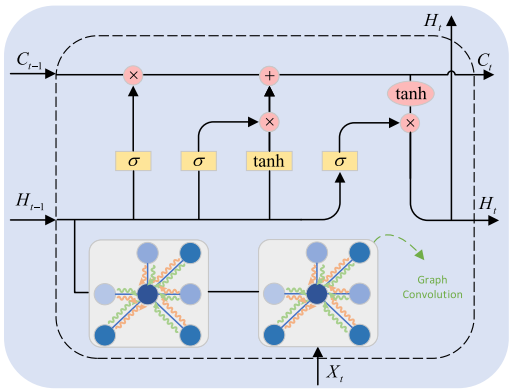

Fig. 6. The structure of the spatio-temporal cell. A two-layer graph convolution operation is added to the input of the original LSTM cell.

$$\hat{Y}_t = (H_t + h_t)W \tag{6}$$

where $\hat{Y}_t$ is the COVID-19 confirmed case prediction result.

Loss Function: In our training process, the goal is to minimize the error between the predicted value and the real COVID-19 confirmed cases. Y_t and $\hat{Y}_t$ represent the real value and the predicted value respectively. The loss function is shown in Formula 7. The first term minimizes the error between the real confirmed case count and the prediction, the second term L_{reg} is the L2 regularization term to avoid overfitting and λ is a hyperparameter.

$$loss = \left(\hat{Y}_t - Y_t\right)^2 + \lambda L_{reg} \tag{7}$$

The prediction model's training and prediction is summarized in Algorithm 1.

D. COVID-19 Risk Stage Evaluation

Decoder Introduction: LSTM can capture the quantitative characteristics of, and trends in, the input. As shown in Fig. 5, the decoder is composed of LSTM, a fully connected layer, and the argmax function. The input $X^e = (X^e_{t-3}, X^e_{t-2}, X^e_{t-1}, X^e_t, \hat{Y}_t)$ includes 4-day historical COVID-19 confirmed cases and the 1-day prediction described above; the output is the current COVID-19 risk stage. The specific formula is as follows:

$$\begin{aligned}
i^e_t &= \sigma\left(W^e_{xi} * X^e + W^e_{hi} * H^e_{t-1} + b^e_i\right) \\
f^e_t &= \sigma\left(W^e_{xf} * X^e + W^e_{hf} * H^e_{t-1} + b^e_f\right) \\
g^e_t &= \tanh\left(W^e_{xg} * X^e + W^e_{hg} * H^e_{t-1} + b^e_g\right) \\
o^e_t &= \sigma\left(W^e_{xo} * X^e + W^e_{ho} * H^e_{t-1} + b^e_o\right) \\
C^e_t &= f^e_t \odot C^e_{t-1} + i^e_t \odot g^e_t \\
H^e_t &= o^e_t \cdot \tanh\left(C^e_t\right)
\end{aligned} \tag{8}$$

where the last H^e_t is the output.

$$Y_{label} = \operatorname{argmax}\left(H^e_t W^e\right) \tag{9}$$

where Y_{label} is the COVID-19 risk stage. The cross-entropy error between evaluation and label is adopted as the loss function.

Data Preparation: In order to prepare for data transfer to solve the problem of data (target data) lack, we first select backup data (source data) that fits the epidemic cycle from the available data (the global COVID-19 confirmed dataset). Specifically, we select countries with $rtm \leq 0.1$ and total confirmed cases greater than 3000 from 187 countries in the global COVID-19 confirmed dataset. The low rtm is considered to represent a complete cycle

Algorithm 1: COVID-19 Confirmed Case Prediction.

Input: Provincial feature matrix X and adjacency matrix A, country feature matrix X_{xf} and the convergence condition ε.
Output: Predicted result Y.

initialize the prediction model(GCNs, LSTM, GRU, fully connected layer) parameters;
initialize $f(X, A) = \emptyset$, learning rate = 0.001, provincial multi-feature representation $H = \emptyset$, country multi-feature representation $h = \emptyset$, $Y = \emptyset$;
Train:
while ε is true **do**
  for each mini batch of training instances **do**
    calculate = $f(X, A)$ based on (3);
    calculate = H based on (4);
    calculate = h based on (5);
    calculate = Y based on (6);
    minimise the loss function $loss$ based on (7);
    update the model parameters;
  end
end
Test:
calculate = $f(X, A)$ based on (3);
calculate = H based on (4);
calculate = h based on (5);
calculate = Y based on (6);
return Y;

Algorithm 2: COVID-19 Data Classification.

Input: All country COVID-19 confirmed data $Data_{All}$ and real risk stage $Tlabel_{All}$, similarity Si.
Output: $category$.

initialize the decoder parameters;
initialize $index = 1$;
while $Data_{All} \neq \emptyset$ **do**
  $category = \emptyset$;
  $Data_{random}$ as input to pre-train decoder;
  for $Data_i$ in $Data_{All}$ **do**
    $Plabel_i = decoder(Data_i)$;
    if $Plabel_i$ and $Tlabel_i$ Si $\geq$ 80% **then**
      $category(index) \leftarrow Data_i$;
      $Data_{All} = Data_{All} - Data_i$;
    end
  end
  index = index + 1;
end
return $category$;

of confirmed COVID-19 cases, and the high case-count threshold reduces the possibility of data errors. We also manually eliminate countries with obvious data errors by analyzing the distribution of data over the COVID-19 confirmed case cycle, and the selected country data is labeled according to the previous rules.

COVID-19 Confirmed Data Classification: Data is classified by comparing the similarity of country data in the embedding space. The classification process is shown in Algorithm 2, and the basic procedures are as follows. We first use a parameter index to record the iterations. In each iteration, a random country's COVID-19 confirmed data $Data_{random}$ is used as the input to pre-train the decoder. This decoder is then used to evaluate all countries' COVID-19 confirmed data $Data_{All}$. If the evaluation label $Plabel_i$ and its real label $Tlabel_i$ exhibit $Si \geq 80$ %, these data are added to $category(index)$. After the classification, these data are divided into six categories, as shown in Table IV.

TABLE IV
COUNTRIES GROUPED BY COVID-19 CONFIRMED CYCLE CHARACTERISTICS

Category	Member	Trends in confirmed caseload
Spain	Spain	From 100 to 2000 in $\leq$ 10 days
Germany	Germany, Italy	From 100 to 1000 in $\leq$ 10 days
Belgium	Belgium	From 100 to 1500 in $\leq$ 20 days
Australia	Australia, Austria, Ireland, Japan, Switzerland	From 100 to 300 in $\leq$ 10 days and 100 to 1000 in $\geq$ 10 days
Finland	Finland, Luxembourg, Norway, Denmark	From 100 to 300 in $\geq$ 10 days
Hungary	Hungary, Thailand	Cases never reach 300

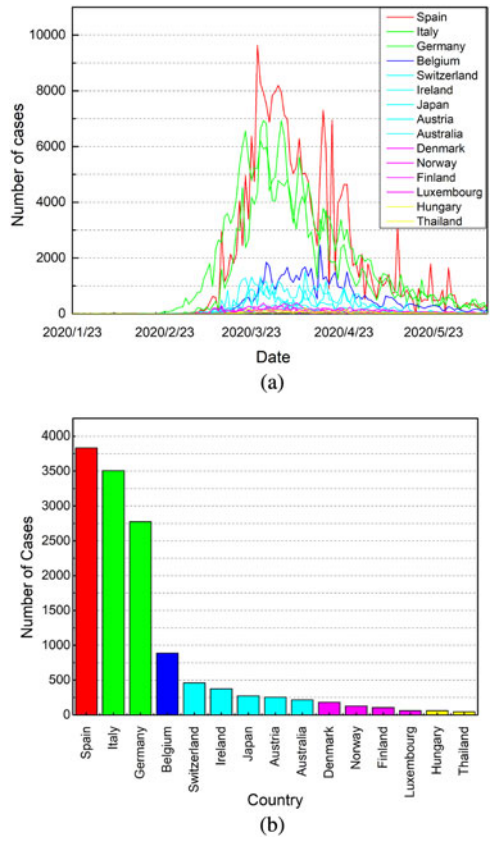

Fig. 7. Data display for various categories. (a) Shows the distribution of different category confirmed data throughout the complete COVID-19 confirmed case cycle. (b) Presents a distribution of all country mean confirmed case count in the complete cycle. Categories are indicated by color.

TABLE V
DESCRIPTION OF COVID-19 FEATURES

		Feature	Description
Province	Basic	Confirmed	Number of the confirmed
		Released	Number of the released
		Deceased	Number of the deceased
	Weather	Avg_temp	Average daily temperature
		Min_temp	Lowest daily temperature
		Max_temp	Highest daily temperature
		Precipitation	Daily precipitation
		Max_wind_speed	Maximum daily wind speed
		Most_wind_direction	Most frequent daily wind direction
		Avg_relative_humidity	Average relative daily humidity
	Geography	Latitude	Latitude of the visit (WGS84)
		Longitude	Longitude of the visit (WGS84)
		Code	Code of the region
	POIs	Elementary_school_count	Number of elementary schools
		Kindergarten_count	Number of kindergartens
		University_count	Number of universities
		Nursing_home_count	Number of nursing homes
		Academy_ratio	Ratio of academies
	Population	Elderly_population	Ratio of the elderly population
		Elderly_alone_ratio	Ratio of elderly households living alone
		Population_count	Population of the province
		Density	Population density
		Sex_bal	Sex balance index
	Policy	level 1-4	Policy of the government
Country	Search trend	Search_interest	Trend data of keywords searched on Naver (an influential South Korean search engine)
	Basic	Confirmed	Number of the confirmed

Category Trend Characteristic Analysis: In Fig. 7, we can see that different categories of data differ mainly in the number of confirmed cases. In Fig. 7(a), countries in the same category have similar COVID-19 cycle changes and distribution. In Fig. 7(b), the average number of confirmed cases in countries in the same category is similar. Thus, we should find trend characteristics in the data of each category, which can help us classify data of unknown category. After combining the epidemic cycle in Fig. 3 and the data analysis results, we obtained these trend characteristics, which are shown in Table IV.

Instance-Based Evaluation: For the same category of data, we can directly transfer the data to solve the problem of lack of data. The direct transfer evaluation process is shown in Algorithm 3, and the basic procedures are summarized as follows. By comparing unknown data trend characteristics Ch_{un} with all categories of data trend characteristics Ch_{All} in Table IV, category data $Data_{category(i)}$ is determined that can be used for transfer. This data is then used to train the decoder. Finally, we use this decoder to evaluate the input X^e and obtain the risk stage evaluation result $Plabel$.

Normalized Instance-Based Evaluation: In Fig. 8, we further propose a normalized data transfer method. This method can use all the data, which it normalizes by dividing the maximum value of each data categories before the decoder is trained. We use the same category normalization approach to normalize South Korea's data. The transfer evaluation process is shown in Algorithm 4. This method greatly improves the accuracy of the evaluation.

V. EXPERIMENTS

A. Data Description

In this section, we evaluate the performance of COV2RS in predicting COVID-19 confirmed cases and evaluating the COVID-19 risk stage on two real-world datasets: South Korea's COVID-19 dataset and a global COVID-19 dataset. Both datasets were obtained from the Kaggle competition–COVID19 Global Forecasting (Week 5: Forecast daily COVID-19 spread in regions around the world) [38]. South Korea's COVID-19 dataset contains multi-feature data; the

Algorithm 3: Instance-Based Evaluation.

Input: All categories' data $Data_{category(All)}$ and trend characteristics Ch_{All}, unknown category data trend characteristics Ch_{un}, decoder input $X^e = (X^e_{t-3}, X^e_{t-2}, X^e_{t-1}, X^e_t, \hat{Y}_t)$.

Output: Risk stage evaluation result $Plabel$.

initialize the decoder parameters;
initialize $Data_{target} = \emptyset$;
initialize $Plabel$ = 0;
for Ch_i in Ch_{All} **do**
  if Ch_i match Ch_{un} **then**
    $Data_{target} \leftarrow Data_{category(i)}$;
  end
end
$Data_{target}$ as input to train decoder;
$Plabel$ = decoder(X^e);
return $Plabel$;

Algorithm 4: Normalized Instance-Based Evaluation.

Input: All country COVID-19 confirmed data $Data_{All}$ and normalization methods N_{All}, all categories' characteristics Ch_{All} and normalization methods $N_{category(All)}$, unknown category data characteristics Ch_{un}, decoder input $X^e = (X^e_{t-3}, X^e_{t-2}, X^e_{t-1}, X^e_t, \hat{Y}_t)$.

Output: Risk stage evaluation result $Plabel$.

initialize the decoder parameters;
initialize $Plabel$ = 0;
for Ch_i in Ch_{All} **do**
  if Ch_i match Ch_{un} **then** $N_{un} = N_{category(i)}$;
  end
end
$N_{All}(Data_{All})$ as input to train decoder;
$Plabel$ = decoder($N_{un}(X^e)$);
return $Plabel$;

global COVID-19 dataset contains country confirmed data from all over the world.

Global Dataset: This dataset contains the COVID-19 confirmed cases, deaths, and recovered cases per day in 187 countries worldwide from 2020/01/22 to 2020/7/21. In the experiment, this dataset is mainly used to transfer data and train the decoder.

South Korea's Dataset: This dataset contains the COVID-19 confirmed cases, deaths, and recovered cases from 2020/01/20 to 2020/06/29 in each of the provinces of South Korea. It also contains weather data (e.g., temperature, precipitation, wind speed), infectious disease alert level, latitude and longitude, population density, proportion of elderly population, number of hospitals, number of schools, total population, COVID-19 search interests, and other relevant data during the COVID-19 outbreak as shown in Table V. In the experiment, we divide these features into provincial and country level representations separately to ascertain the spatio-temporal dependence. South Korea has 17 provinces; thus, a 17 × 17 adjacency matrix A describes the spatial relationship between provinces. Each row represents a province, and the values in matrix A represent the connectivity between provinces. The

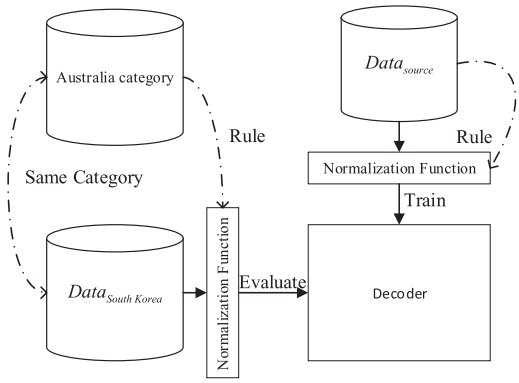

Fig. 8. Normalized data transfer method.

feature matrix X describes the changes in all features over time. The 17 rows represent 17 provinces, and the 24 columns represent values for the 24 features.

In the experiment, we normalized all features to the interval [0, 1]. Furthermore, in the COVID-19 confirmed case prediction portion, 70% of the data is used as the training set, 15% as the validation set, and the remaining 15% as the test set. The prediction interval is one day, and the prediction result is combined with 4 historical country-level daily confirmed case counts as decoder input to evaluate the COVID-19 risk stage. In the decoder training phase, the training set is obtained through data transfer from other similar countries, and South Korea's COVID-19 confirmed case data is used as the test set.

B. Evaluation Metrics

We use three indicators to evaluate the performance of the COV2RS prediction results, and one indicator to evaluate the performance of the COV2RS evaluation results.

(1) Root Mean Squared Error (RMSE):

$$RMSE = \sqrt{\frac{1}{M}\sum_{t=1}^{M}(y_t - \hat{y}_t)^2} \tag{10}$$

(2) Mean Absolute Error (MAE):

$$MAE = \frac{1}{M}\sum_{t=1}^{M}|(y_t - \hat{y}_t)| \tag{11}$$

(3) Acc_{tend}:

$$Acc_{tend} = \frac{n_{True\_tend\_day}}{n_{All\_day}} \tag{12}$$

(4) Accuracy:

$$Accuracy = \frac{n_{right}}{n_{sum}} \tag{13}$$

where y represents the real COVID-19 confirmed cases and $\hat{y}$ represents the predicted case count. M is the number of sampling times. $n_{True\_tend\_day}$ represents the number of correct tendency prediction days, and n_{All_day} is the total number of tendency prediction days. Similarly, n_{right} is the number of

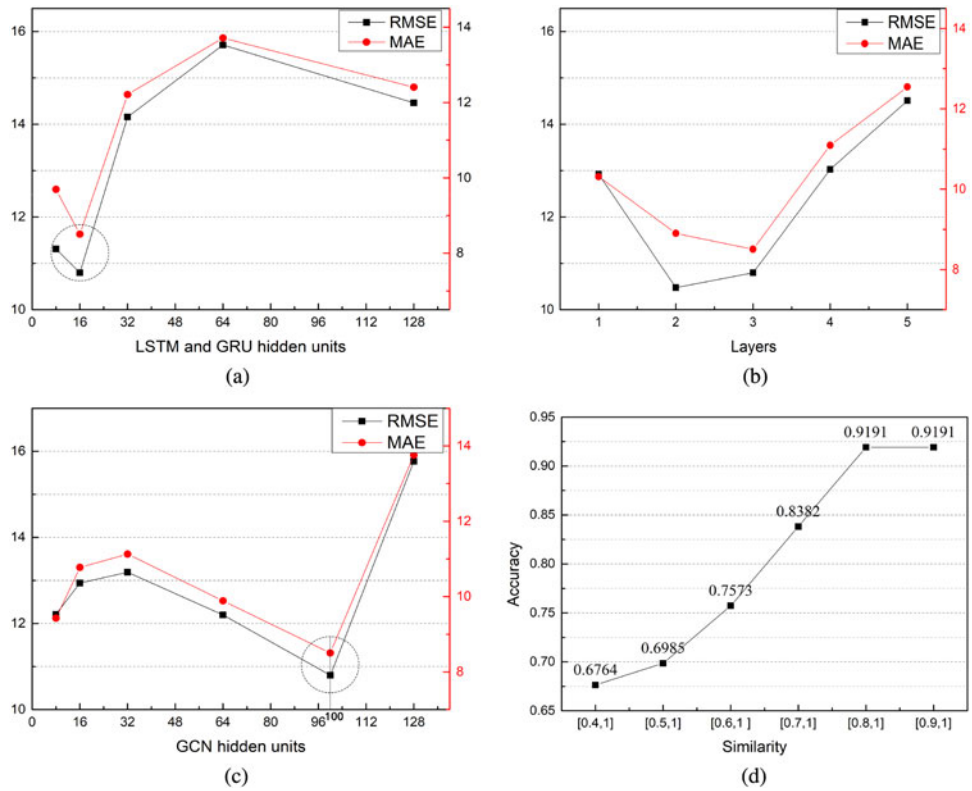

Fig. 9. Influence of different model parameters on prediction and evaluation results. (a)-(c) Show the influence of different numbers of LSTM and GRU hidden units (a), LSTM and GRU layers (b), and GCN units (c) on COVID-19 confirmed case prediction errors. (d) Shows the influence of different similarity (Si) standards on COVID-19 risk stage evaluation accuracy.

correct risk stage evaluation days, and n_{sum} is the total number of days for risk stage evaluation.

Specifically, RMSE and MAE are used to measure prediction errors: the smaller the value, the better the prediction effect. Acc_{tend} represents the model's accuracy in predicting the COVID-19 case count tendency, which can help us to understand the short-term direction of the epidemic's development. Accuracy is used to measure evaluation accuracy: a larger value denotes a better prediction effect.

C. Choosing Model Parameters

Hyperparameters: In this section, we select the relevant parameters of COV2RS.

The main hyperparameters of COVID-19 prediction include: batch size, learning rate, training epoch, number of LSTM and GRU hidden units, number of GCN hidden units, and number of LSTM layers. For this experiment, we manually adjusted the batch size to 32, the learning rate to 0.001, and the training epoch to 2500.

The number of LSTM and GRU hidden units and layers, and of GCN hidden units, are important parameters for COVID-19 prediction: different numbers have a huge impact on prediction precision. We test a variety of numbers and select the best value by comparing prediction precision.

In our experiment, we choose the number of LSTM and GRU hidden units from [8, 16, 32, 64, 128] and analyze the change in COVID-19 prediction precision. In Fig. 9(a), the vertical axis represents the change in RMSE and MAE results, and the horizontal axis represents the number of hidden units. It can be seen that the result is best with 16 hidden units; as the number of hidden units is increased, the error indicators first fall, then rise. This is mainly because increases in the number of hidden units greatly increase the model complexity and computational difficulty, and overfitting arises on the training data. Thus, we set the number of hidden units to 16.

Similarly, we choose the number of LSTM and GRU layers from [1, 2, 3, 4, 5] and GCN units from [8, 16, 32, 64, 100, 128] and again analyze the change in prediction precision. Based on the precision levels reported in Figs. 9(b) and 9(c), we set the number of GCN hidden units to 100 and LSTM and GRU layers to 3.

The major hyperparameters for risk stage evaluation include: batch size, learning rate, training epoch, number of hidden units, and number of layers. For the purposes of this experiment, we manually adjusted the batch size to 32, the learning rate to 0.001, the number of hidden units to 50, and the number of the layers to 3. These hyperparameters have an impact on the training efficiency of the decoder but have little effect on the decoder's evaluation accuracy.

The standard of similarity (Si) in the COVID-19 Data Classification Algorithm is a very important parameter for the evaluation accuracy of the decoder. We used Austria's COVID-19 confirmed case data as pre-training data; evaluation results are shown in Fig. 10. We choose the Si from [0.4, 0.5, 0.6, 0.7, 0.8, 0.9] and analyze the change in COVID-19

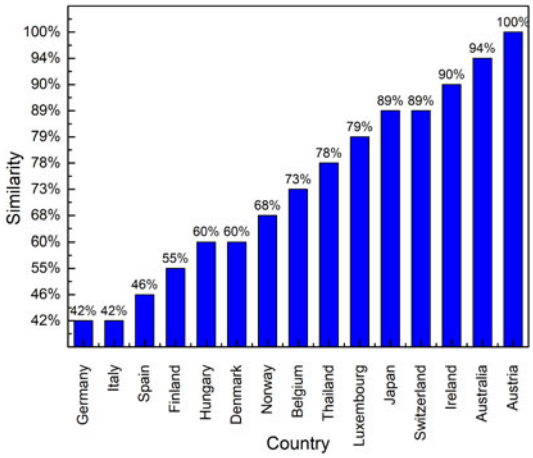

Fig. 10. Characteristic similarity between different countries.

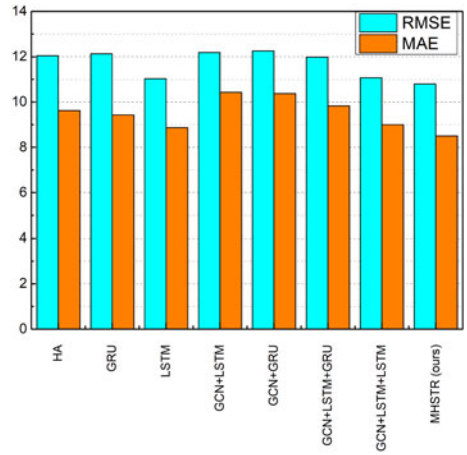

Fig. 11. Comparison of model prediction results.

TABLE VI
PREDICTION RESULTS ON THE SOUTH KOREA DATASET

Metric	RMSE	MAE	Acc_{tend}
HA	12.044	9.627	52.38%
GRU	12.128	9.432	47.62%
LSTM	11.026	8.87	61.90%
GCN+LSTM	12.180	10.432	47.62%
GCN+GRU(T-GCN)	12.259	10.373	47.62%
GCN+LSTM+GRU	11.980	9.829	57.14%
GCN+LSTM+LSTM	11.070	9.001	**66.67%**
MHSTR (ours)	**10.797**	**8.505**	**66.67%**

evaluation precision. As shown in Fig. 9(d), different Si selection standards exert a significant influence on the final evaluation accuracy. There, the vertical axis represents the COVID-19 risk stage evaluation accuracy, and the horizontal axis represents Si standards. It can be seen that increasing Si also increases the evaluation accuracy; the more similar the data is, the more important it is to the experimental results. For the convenience of the experiment, the Si standard was set to 80%.

Training: In COVID-19 confirmed case prediction, 70% of the South Korea dataset is used as the training set, 15% as the validation set, and the remaining 15% as the test set. In COVID-19 risk stage evaluation, we set the training set and test set flexibly. We use gradient descent and the Adam optimizer as the optimization method during training.

D. Experimental Results

We use our model to predict and evaluate COVID-19. We use our model to evaluate Ebola.

COVID-19: We compare the performance of COV2RS's confirmed case prediction with the following baseline methods: the History Average model (HA), which uses historical averages of COVID-19 confirmed cases as the prediction; LSTM [39]; GRU [40]; T-GCN [41]; and single-feature hierarchical spatio-temporal representation models (GCN +LSTM+LSTM, GCN+LSTM+GRU), which use single features from our multi-feature hierarchical spatio-temporal representation (MHSTR) prediction.

Table VI and Fig. 11 show the performance of the MHSTR prediction method and other baseline methods for the forecasting task on the South Korea dataset. The MHSTR prediction method obtain the best prediction performance under all evaluation metrics for all prediction horizons. We also find that direct spatio-temporal dependence in a single layer on a single feature did not obtain good prediction results; the RMSE and MAE errors of the GCN+LSTM method were 10.47% and 17.61% higher than LSTM method, and the corresponding errors of the T-GCN method were 1.08% and 9.98% higher than the GRU method. Furthermore, the GCN+LSTM+LSTM method is basically the same as the MHSTR model, except that the GRU portion is changed to LSTM and the input is a single feature. Compared with the GCN+LSTM method, this method shows 9.11% and 13.72% decreases in RMSE and MAE, respectively; this indicates that the hierarchical model played a key role in prediction accuracy. Finally, our MHSTR model reduced the errors by 2.47% and 5.51% over the GCN +LSTM+LSTM method, and by 2.08% and 4.11% compared with the optimal baseline LSTM method. Overall, compared with these baselines, our method achieved the highest accuracy in determining COVID-19 epidemic trends. The experimental results prove that a multi-feature hierarchical spatio-temporal representation method plays a key role in COVID-19 confirmed case prediction. In this part, we tried cross-validation, but there are two problems: 1. The model is a two-layer model. The model input consists of four parts and contains 26 features. It is difficult to use cross-validation. 2. The chronological order of COVID-19 confirmed data is very important, and cross-validation breaks the chronological order, which is not good for the experiment. Therefore, cross-validation was not used in the experiment.

Table VII shows the COVID-19 risk stage evaluation accuracy of the different data transfer methods in different countries. We calculated 90% confidence interval (CI). The

TABLE VII
COVID-19 RISK STAGE EVALUATION ACCURACY OF DIFFERENT DATA TRANSFER METHODS

	South Korea		Australia		Austria	
Method	Source Data	Accuracy	Source data	Accuracy	Source data	Accuracy
Instance-based evaluation	Australia category (31.25% data)	91.91±3.78%	Australia category (31.25% data)	91.91±3.78%	Australia category (31.25% data)	93.38±3.45%
Normalized instance-based evaluation	31.25% data	94.85±3.06%	31.25% data	92.65±3.62%	31.25% data	93.38±3.45%
	50% data	97.06±2.34%	50% data	94.85±3.06%	50% data	96.32±2.61%
	100% data	**97.79±2.04%**	100% data	**97.79±2.04%**	100% data	**97.06±2.34%**
	Ireland		Japan		Switzerland	
Method	Source Data	Accuracy	Source data	Accuracy	Source data	Accuracy
Instance-based evaluation	Australia category (31.25% data)	92.65±3.62%	Australia category (31.25% data)	92.65±3.62%	Australia category (31.25% data)	90.44±4.08%
Normalized instance-based evaluation	31.25% data	90.44±4.08%	31.25% data	91.91±3.78%	31.25% data	88.97±4.34%
	50% data	90.44±4.08%	50% data	93.38±3.45%	50% data	91.91±3.78%
	100% data	**93.38±3.45%**	100% data	**94.12±3.26%**	100% data	**94.12±3.26%**
	Finland		Luxembourg		Norway	
Method	Source Data	Accuracy	Source data	Accuracy	Source data	Accuracy
Instance-based evaluation	Finland category (18.75% data)	83.82±5.10%	Finland category (18.75% data)	86.76±4.70%	Finland category (18.75% data)	83.09±5.20%
Normalized instance-based evaluation	18.75% data	91.91±3.78%	18.75% data	91.18±3.93%	18.75% data	86.76±4.70%
	50% data	91.18±3.93%	50% data	92.65±3.62%	50% data	**90.44±4.08%**
	100% data	**92.65±3.62%**	100% data	**93.38±3.45%**	100% data	**90.44±4.08%**

TABLE VIII
EBOLA RISK STAGE EVALUATION ACCURACY

	Normalized instance-based evaluation	
Country	Source Data	Accuracy
Liberia	Guinea, Sierra Leone	98.00±1.85%
Guinea	Liberia, Sierra Leone	98.42±1.27%
Sierra Leone	Liberia, Guinea	98.02±1.42%

"Source Data" field represents the training data and its utilization of the source data. If the country's COVID-19 data has gone through the complete SIR model process (epidemic confirmed cycle), the data can be added to the source data.

The experimental results show that the instance-based evaluation method performs well and has 31.25%/18.75% utilization of the source data. The normalized instance-based evaluation method further improves the accuracy of risk stage evaluation and utilizes up to 100% of the source data. The accuracy of COVID-19 risk stage evaluation can reach up to 97.79%. And almost all experimental results show that the best evaluation results are obtained when the normalized instance-based evaluation method is used and the data utilization rate reaches 100%. The same-country source data attains results that are comparable to if not inferior to cross-country transfer at 100%. The key reason for this problem lies in the normalization of data. The same-country source data, without data normalization processing, will retain the size characteristics of the data, which helps

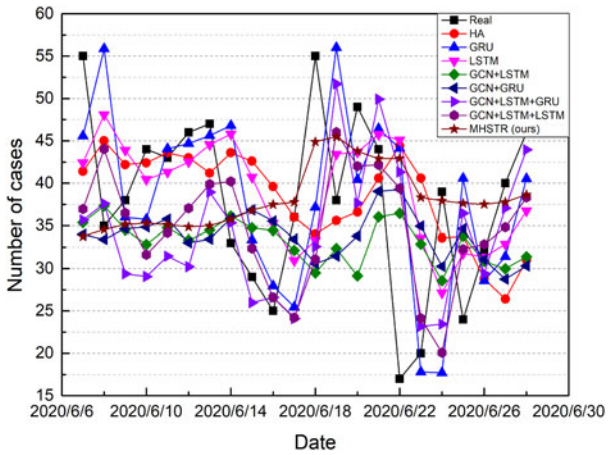

Fig. 12. Visual display of prediction results. It shows the visualization of the COVID-19 confirmed case prediction results. Compared with baselines, our model avoids the lagging problem and attains the best prediction results.

to improve the accuracy of the experiment. However, due to the limited amount of same-country data, it is not enough to cover the feature space, resulting in low experimental accuracy. Cross-country data, through the normalization operation, solves this problem. Therefore, for the same-country source data, no normalization operation always has better experimental results than the normalization operation, but there are exceptions, which are caused by the randomness of the normalization operation. In general, in the case of using cross-country data,

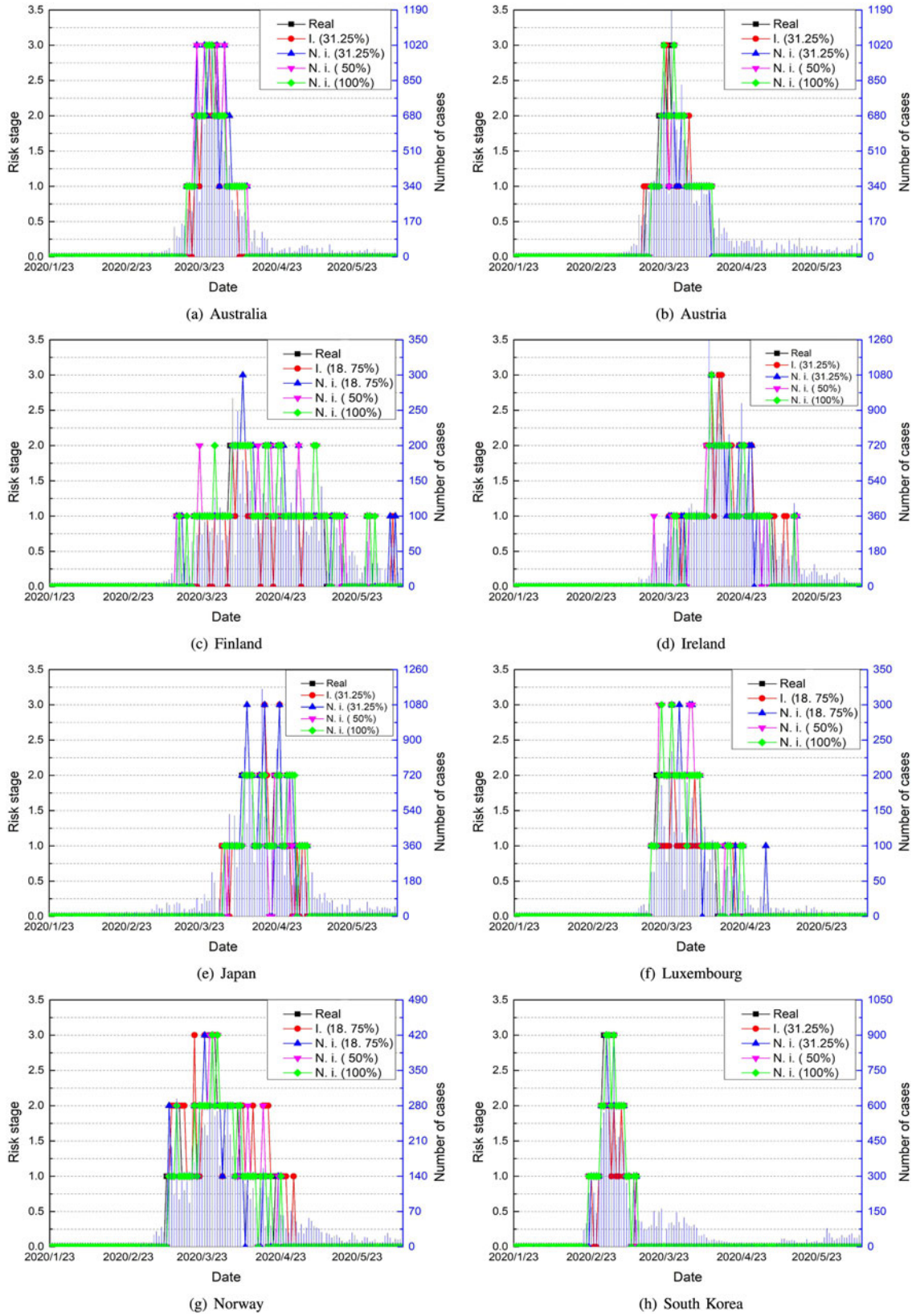

Fig. 13. Visual display of evaluation results. It shows the visualization of the COVID-19 risk stage evaluation results of different transfer methods in different countries. "Real" represents the real COVID-19 risk stage. "I. (31.25%)" represents the instanced-based evaluation results under the use of 31.25% of the source data. "I. (18.75%)" represents the instanced-based evaluation results under the use of 18.75% of the source data. "N. I. (31.25%)" represents the normalized instanced-based evaluation results under the use of 31.25% of the source data. "N. I. (18.75%)" represents the normalized instanced-based evaluation results under the use of 18.75% of the source data. "N. I. (50%)" represents the normalized instanced-based evaluation results under the use of 50% of the source data. "N. I. (100%)" represents the normalized instanced-based evaluation results under the use of 100% of the source data.

TABLE IX
EVALUATION DATA T-TEST RESULTS $statistic(pvalue)$

	Australia	Austria	Ireland	Japan	South Korea	Switzerland		Denmark	Finland	Luxembourg	Norway
Australia	0.0(1.00E+00)	0.7(4.93E-01)	2.7(7.56E-03)	1.1(2.79E-01)	0.9(3.80E-01)	3.4(8.27E-04)	Denmark	0.0(1.00E+00)	4.1(5.91E-05)	6.5(3.14E-10)	2.5(1.46E-02)
Austria	0.7(4.93E-01)	0.0(1.00E+00)	2.0(4.14E-02)	0.4(7.03E-01)	1.6(1.05E-01)	2.9(4.64E-03)	Finland	4.1(5.91E-05)	0.0(1.00E+00)	3.3(1.07E-03)	1.3(1.94E-01)
Ireland	2.7(7.56E-03)	2.0(4.14E-02)	0.0(1.00E+00)	1.7(8.54E-02)	3.7(2.79E-04)	1.1(2.71E-01)	Luxembourg	6.5(3.14E-10)	3.3(1.07E-03)	0.0(1.00E+00)	3.9(1.35E-04)
Japan	1.1(2.79E-01)	0.4(7.03E-01)	1.7(8.54E-02)	0.0(1.00E+00)	2.1(3.76E-02)	2.6(1.00E-02)	Norway	2.5(1.46E-02)	1.3(1.94E-01)	3.9(1.35E-04)	0.0(1.00E+00)
South Korea	0.9(3.80E-01)	1.6(1.05E-01)	3.7(2.79E-04)	2.1(3.76E-02)	0.0(1.00E+00)	4.2(4.21E-05)		Germany			Thailand
Switzerland	3.4(8.27E-04)	2.9(4.64E-03)	1.1(2.71E-01)	2.6(1.00E-02)	4.2(4.21E-05)	0.0(1.00E+00)	Italy	1.6(1.07E-01)		Hungary	1.5(1.44E-01)

TABLE X
NORMALIZED EVALUATION DATA T-TEST RESULTS $statistic(pvalue)$

	Australia	Austria	Belgium	Denmark	Finland	Germany	Hungary	Ireland	Italy	Japan	South Korea	Luxembourg	Norway	Spain	Switzerland	Thailand
Australia	0.0(1.00E+00)	0.6(5.58E-01)	2.7(7.11E-03)	4.5(1.08E-05)	3.4(8.48E-04)	3.1(2.02E-03)	1.4(1.56E-01)	0.6(5.39E-01)	5.2(4.57E-07)	0.3(7.30E-01)	0.2(8.40E-01)	0.7(4.69E-01)	2.1(3.37E-02)	3.1(2.36E-03)	2.2(2.93E-02)	0.6(5.75E-01)
Austria	0.6(5.58E-01)	0.0(1.00E+00)	3.6(4.25E-04)	5.4(1.12E-07)	4.3(2.08E-05)	3.9(1.31E-04)	2.3(2.35E-02)	1.3(1.80E-01)	6.0(5.31E-09)	1.0(3.06E-01)	0.4(6.84E-01)	1.4(1.77E-01)	2.9(3.74E-03)	3.8(1.63E-04)	2.9(4.64E-03)	1.2(2.25E-01)
Belgium	2.7(7.11E-03)	3.6(4.25E-04)	0.0(1.00E+00)	1.8(6.61E-02)	0.6(5.56E-01)	0.7(5.11E-01)	1.6(1.18E-01)	2.3(2.12E-02)	2.8(5.70E-03)	2.5(1.16E-02)	3.1(2.33E-03)	1.9(5.99E-02)	0.6(2.81E-01)	0.6(5.35E-01)	0.2(8.45E-01)	2.2(3.01E-02)
Denmark	4.5(1.08E-05)	5.4(1.12E-07)	1.8(6.61E-02)	0.0(1.00E+00)	1.3(1.90E-01)	1.0(2.95E-01)	3.5(4.92E-04)	4.2(3.32E-05)	1.1(2.77E-01)	4.4(1.48E-05)	4.9(1.50E-06)	3.6(3.40E-04)	2.4(1.85E-02)	1.1(2.83E-01)	1.8(6.71E-02)	4.0(8.72E-05)
Finland	3.4(8.48E-04)	4.3(2.08E-05)	0.6(5.56E-01)	1.3(1.90E-01)	0.0(1.00E+00)	0.1(8.92E-01)	2.3(2.41E-02)	3.0(2.70E-03)	2.3(2.10E-02)	3.2(1.33E-03)	3.8(1.85E-04)	2.5(1.29E-02)	1.2(2.51E-01)	0.1(9.19E-01)	0.7(4.73E-01)	2.8(4.92E-03)
Germany	3.1(2.02E-03)	3.9(1.31E-04)	0.7(5.11E-01)	1.0(2.95E-01)	0.1(8.92E-01)	0.0(1.00E+00)	2.1(3.58E-02)	2.8(5.95E-03)	2.0(4.62E-02)	3.0(3.26E-03)	3.4(6.62E-04)	2.4(1.87E-02)	1.2(2.48E-01)	0.0(9.76E-01)	0.8(4.39E-01)	2.6(8.80E-03)
Hungary	1.4(1.56E-01)	2.3(2.35E-02)	1.6(1.18E-01)	3.5(4.92E-04)	2.3(2.41E-02)	2.1(3.58E-02)	0.0(1.00E+00)	0.9(3.80E-01)	4.3(2.08E-05)	1.2(2.50E-01)	1.8(7.96E-02)	0.6(5.74E-01)	0.9(3.45E-01)	2.1(4.01E-02)	1.1(2.54E-01)	0.8(4.13E-01)
Ireland	0.6(5.39E-01)	1.3(1.80E-01)	2.3(2.12E-02)	4.2(3.32E-05)	3.0(2.70E-03)	2.8(5.95E-03)	0.9(3.80E-01)	0.0(1.00E+00)	4.9(1.34E-06)	0.3(7.76E-01)	0.9(3.78E-01)	0.2(8.47E-01)	1.7(9.05E-02)	2.7(6.89E-03)	1.8(7.32E-02)	0.0(9.89E-01)
Italy	5.2(4.57E-07)	6.0(5.31E-09)	2.8(5.70E-03)	1.1(2.77E-01)	2.3(2.10E-02)	2.0(4.62E-02)	4.3(2.08E-05)	4.9(1.34E-06)	0.0(1.00E+00)	5.1(6.07E-07)	5.6(6.36E-08)	4.4(1.63E-05)	3.3(1.27E-03)	2.0(4.39E-02)	2.7(7.08E-03)	4.7(3.76E-06)
Japan	0.3(7.30E-01)	1.0(3.06E-01)	2.5(1.16E-02)	4.4(1.48E-05)	3.2(1.33E-03)	3.0(3.26E-03)	1.2(2.50E-01)	0.3(7.76E-01)	5.1(6.07E-07)	0.0(1.00E+00)	0.6(5.57E-01)	0.4(6.61E-01)	1.9(5.48E-02)	2.9(3.81E-03)	2.0(4.64E-02)	0.2(8.03E-01)
South Korea	0.2(8.40E-01)	0.4(6.84E-01)	3.1(2.33E-03)	4.9(1.50E-06)	3.8(1.85E-04)	3.4(6.62E-04)	1.8(7.96E-02)	0.9(3.78E-01)	5.6(6.36E-08)	0.6(5.57E-01)	0.0(1.00E+00)	1.0(3.38E-01)	2.5(1.45E-02)	3.4(7.96E-04)	2.5(1.44E-02)	0.8(4.24E-01)
Luxembourg	0.7(4.69E-01)	1.4(1.77E-01)	1.9(5.99E-02)	3.6(3.40E-04)	2.5(1.29E-02)	2.4(1.87E-02)	0.6(5.74E-01)	0.2(8.47E-01)	4.4(1.63E-05)	0.4(6.61E-01)	1.0(3.38E-01)	0.0(1.00E+00)	1.3(1.82E-01)	2.3(2.09E-02)	1.5(1.44E-02)	0.2(8.47E-01)
Norway	2.1(3.37E-02)	2.9(3.74E-03)	0.6(5.81E-01)	2.4(1.85E-02)	1.2(2.51E-01)	1.2(2.48E-01)	0.9(3.45E-01)	1.7(9.05E-02)	3.3(1.27E-03)	1.9(5.48E-02)	2.5(1.45E-02)	1.3(1.82E-01)	0.0(1.00E+00)	1.1(2.64E-01)	0.3(7.68E-01)	1.6(1.10E-01)
Spain	3.1(2.36E-03)	3.8(1.63E-04)	0.6(5.35E-01)	1.1(2.83E-01)	0.1(9.19E-01)	0.0(9.76E-01)	2.1(4.01E-02)	2.7(6.89E-03)	2.0(4.39E-02)	2.9(3.81E-03)	3.4(7.96E-04)	2.3(2.09E-02)	1.1(2.64E-01)	0.0(1.00E+00)	0.7(4.59E-01)	2.6(1.00E-02)
Switzerland	2.2(2.93E-02)	2.9(4.63E-03)	0.2(8.45E-01)	1.8(6.71E-02)	0.7(4.73E-01)	0.8(4.39E-01)	1.1(2.54E-02)	1.8(7.32E-02)	2.7(7.08E-03)	2.0(4.64E-02)	2.5(1.44E-02)	1.5(1.38E-01)	0.3(7.68E-01)	0.7(4.59E-01)	0.0(1.00E+00)	1.7(8.66E-02)
Thailand	0.6(5.75E-01)	1.2(2.25E-01)	2.2(3.01E-02)	4.0(8.72E-05)	2.8(4.92E-03)	2.6(8.80E-03)	0.8(4.13E-01)	0.0(9.89E-01)	4.7(3.76E-06)	0.2(8.03E-01)	0.8(4.24E-01)	0.2(8.47E-01)	1.6(1.10E-01)	2.6(1.00E-02)	1.7(8.66E-02)	0.0(1.00E+00)

when the amount of data is sufficient to cover the feature space, the optimal evaluation results can always be obtained with the highest data utilization rate.

When training different methods, the running time of different methods is related to the size of the training source data. The time complexity of model training is $O(n^a)$, where a is the number of training times. The more source data n, the longer the training time of the model. The time complexity of model prediction is $O(n)$. If the country's COVID-19 data has gone through the complete SIR model process (epidemic confirmed cycle), the data can be added to the source data.

Ebola: We select Ebola's confirmed data from Liberia, Guinea and Sierra Leone from August 2014 to March 2016 and use our methods for evaluation (Ebola confirmed data in other countries is insufficient). The evaluation results are shown in the Table VIII. We calculated 90% confidence interval. The SIR model can be applied to the diffusion of the Ebola epidemic, and the existing Ebola epidemic data has also gone through the complete SIR model process. So, we can use our model to evaluate Ebola. Good experimental results prove the effectiveness of the experimental method. Our model can evaluate all epidemics that fit the SIR model and have gone through the complete SIR model process.

E. Model Interpretation

To better understand our model, we visualize the results of the COVID-19 confirmed case prediction and COVID-19 risk stage evaluation.

From Fig. 12, we can see that the baselines exhibit large errors between predicted and real values. This is because the baselines are based on a single feature, so the prediction results are always one-sided and lagging. Our model adopts multi-feature data and captures COVID-19 data's spatio-temporal dependence to solve this problem. In Fig. 13, we analyze the transfer effect of different data transfer methods in different countries. The COVID-19 risk stage evaluation results are highly consistent with the true value. In addition, in order to enhance the interpretability of the evaluation model, we conducted t-test on the data of all countries participating in the evaluation. The test results $statistic(pvalue)$ in Table IX show that there is a connection between the data, and the data classification results in our experiment are basically in line with the t-test results, but there will be divergence on the classification boundary. For example, according to our algorithm, Denmark is classified in the Finland country category, and the t-test results show that there are significant differences between Denmark and other data of this category. Table IX explains why the instance-based evaluation method is effective. Table IX and Table X further show that the normalized data greatly increases the similarity between the data and explain why the normalized instance-based evaluation method is effective.

VI. CONCLUSION

In this paper, we propose COV2RS, a COVID-19 prediction and evaluation model. The novel contribution of this paper is predominantly application, and this contribution is based on model innovation and algorithm innovation. The design of the model and algorithm realizes the prediction and evaluation of the SARS-Cov-2. The proposed model is divided into three parts: multi-feature hierarchical spatio-temporal representation, COVID-19 confirmed case prediction, and COVID-19 risk stage evaluation. Our chosen representation strategy can capture COVID-19 multiple features by analyzing the spatio-temporal dependence of data at the provincial and country level. Case prediction is based on this representation, whose results are hierarchically aggregated to obtain confirmed case prediction results. Then, we transfer data from other countries to train the decoder and combine with the prediction result for evaluation results. Experimental results show that our model

can achieve better prediction results in COVID-19 confirmed case prediction than baseline methods and can accurately evaluate the COVID-19 risk stage. This evaluation method starts from the epidemic confirmed cycle and can solve similar problems. This study is our attempt to address the severe and ongoing problems brought by COVID-19 from the perspective of data. With it, we hope to provide a new perspective to understand this epidemic and contribute to the solution of some practical problems.

ACKNOWLEDGMENT

The authors would like to thank Pengfei Li from the School of Computer Science and Technology, Zhejiang University of Technology, China, for his help with the experiments. They also like to thank researchers from all over the world who actively contributed to the Kaggle competition COVID19—Global Forecasting (Week 5: Forecast daily COVID-19 spread in regions around the world), and the global COVID-19 dataset support provided by this competition. Among them, the [COVID-19] EDA (S. Korea) | Forecasting (Global) research work has inspired the authors. Rhey would also like to thank Jihoo Kim, M.S. from the Computer Science department at Hanyang University Seoul, Seoul, South Korea, for sharing the South Korea's dataset on Kaggle.

REFERENCES

[1] W. Kuo and J. He, "Guest Editorial: Crisis management–from nuclear accidents to outbreaks of COVID-19 and infectious diseases," *IEEE Trans. Rel.*, vol. 69, no. 3, pp. 846–850, Sep. 2020.

[2] Y. C. Chen, P. E. Lu, C. S. Chang, and T. H. Liu, "A time-dependent SIR model for COVID-19 with undetectable infected persons," *IEEE Trans. Netw. Sci. Eng.*, vol. 7, no. 4, pp. 3279–3294, Oct.–Dec. 2020.

[3] A. Mourad, A. Srour, H. Harmanai, C. Jenainati, and M. Arafeh, "Critical impact of social networks infodemic on defeating coronavirus COVID-19 pandemic: Twitter-based study and research directions," *IEEE Trans. Netw. Serv. Manage.*, vol. 17, no. 4, pp. 2145–2155, Dec. 2020.

[4] L. Li *et al.*, "Characterizing the propagation of situational information in social media during COVID-19 epidemic: A case study on Weibo," *IEEE Trans. Comput. Soc. Syst.*, vol. 7, no. 2, pp. 556–562, Apr. 2020.

[5] N. Zheng *et al.*, "Predicting COVID-19 in China using hybrid AI model," *IEEE Trans. Cybern.*, vol. 50, no. 7, pp. 2891–2904, Jul. 2020.

[6] M. Bannister-Tyrrell, A. Meyer, C. Faverjon, and A. Cameron, "Preliminary evidence that higher temperatures are associated with lower incidence of COVID-19, for cases reported globally up to 29th february 2020," *medRxiv*, 2020, doi: 10.1101/2020.03.18.20036731.

[7] M. M. Sajadi, P. Habibzadeh, A. Vintzileos, S. Shokouhi, F. Miralles-Wilhelm, and A. Amoroso, "Temperature, humidity, and latitude analysis to estimate potential spread and seasonality of coronavirus disease 2019 (COVID-19)," *JAMA Netw. Open*, vol. 3, no. 6, p. e2011834, 2020, doi: 10.1001/jamanetworkopen.2020.11834.

[8] J. H. Buckner, G. Chowell, and M. R. Springborn, "Dynamic prioritization of COVID-19 vaccines when social distancing is limited for essential workers," *Proc. Nat. Acad. Sci. USA*, vol. 118, no. 16, p. e2025786118, 2021, doi: 10.1073/pnas.2025786118.

[9] X. Kong *et al.*, "Real-time mask identification for COVID-19: An edge computing-based deep learning framework," *IEEE Internet Things J.*, vol. 8, no. 21, pp. 15929–15938, Nov. 2021.

[10] F. Schlosser *et al.*, "COVID-19 lockdown induces disease-mitigating structural changes in mobility networks," in *Proc. Nat. Acad. Sci. USA*, Jan. 2022, pp. 2883–32890.

[11] V. La Gatta, V. Moscato, M. Postiglione, and G. Sperli, "An epidemiological neural network exploiting dynamic graph structured data applied to the COVID-19 outbreak," *IEEE Trans. Big Data*, vol. 7, no. 1, pp. 45–55, Mar. 2021.

[12] G. Dudas *et al.*, "Virus genomes reveal factors that spread and sustained the Ebola epidemic," *Nature*, vol. 544, no. 7650, pp. 309–315, 2017.

[13] N. R. Faria *et al.*, "Establishment and cryptic transmission of Zika virus in Brazil and the Americas," *Nature*, vol. 546, no. 7658, pp. 406–410, 2017.

[14] M. Salehi, R. Sharma, M. Marzolla, M. Magnani, P. Siyari, and D. Montesi, "Spreading processes in multilayer networks," *IEEE Trans. Netw. Sci. Eng.*, vol. 2, no. 2, pp. 65–83, Apr.–Jun. 2015.

[15] J. O. Wertheim *et al.*, "The global transmission network of HIV-1," *J. Infect. Dis.*, vol. 209, no. 2, pp. 304–313, 2014.

[16] J. Ginsberg, M. H. Mohebbi, R. S. Patel, L. Brammer, M. S. Smolinski, and L. Brilliant, "Detecting influenza epidemics using search engine query data," *Nature*, vol. 457, no. 7232, pp. 1012–1014, 2009.

[17] S. Yang, M. Santillana, and S. C. Kou, "Accurate estimation of influenza epidemics using Google search data via ARGO," *Proc. Nat. Acad. Sci. USA*, vol. 112, no. 47, pp. 14473–14478, 2015.

[18] B. T. Grenfell *et al.*, "Unifying the epidemiological and evolutionary dynamics of pathogens," *Science*, vol. 303, no. 5656, pp. 327–332, 2004.

[19] C. Schmidt, "Real-time flu tracking," *Nature*, vol. 573, no. 7774, pp. S58–S58, 2019.

[20] K. Xu, W. Hu, J. Leskovec, and S. Jegelka, "How powerful are graph neural networks?," in *Proc. Int. Conf. Learn. Representations*, 2018.

[21] G. Shen, Z. Zhao, and X. Kong, "GCN2CDD: A commercial district discovery framework via embedding space clustering on graph convolution networks," *IEEE Trans. Ind. Informat.*, vol. 18, no. 1, pp. 356–364, Jan. 2022.

[22] Z. Zhang, P. Cui, and W. Zhu, "Deep learning on graphs: A survey," *IEEE Trans. Knowl. Data Eng.*, vol. 34, no. 1, pp. 249–270, Jan. 2022.

[23] R. Fu, Z. Zhang, and L. Li, "Using LSTM and GRU neural network methods for traffic flow prediction," in *Proc. 31st Youth Academic Annu. Conf. Chin. Assoc. Automat.*, Wuhan, China, 2016, pp. 324–328.

[24] Y. Seo, M. Defferrard, P. Vandergheynst, and X. Bresson, "Structured sequence modeling with graph convolutional recurrent networks," in *Proc. Neural Inf. Process. Syst.*, Cham, Switzerland, Springer, 2018, pp. 362–373.

[25] C. Si, W. Chen, W. Wang, L. Wang, and T. Tan, "An attention enhanced graph convolutional LSTM network for skeleton-based action recognition," in *Proc. IEEE/CVF Conf. Comput. Vis. Pattern Recognit.*, 2019, pp. 1227–1236.

[26] S. Yan, Y. Xiong, and D. Lin, "Spatial temporal graph convolutional networks for skeleton-based action recognition," in *Proc. AAAI Conf. Artif. Intell.*, 2018, pp. 1–9.

[27] S. J. Pan and Q. Yang, "A survey on transfer learning," *IEEE Trans. Knowl. Data Eng.*, vol. 22, no. 10, pp. 1345–1359, Oct. 2010.

[28] M. Sugiyama, T. Suzuki, S. Nakajima, H. Kashima, P. von Bünau, and M. Kawanabe, "Direct importance estimation for covariate shift adaptation," *Ann. Inst. Statist. Math.*, vol. 60, no. 4, pp. 699–746, 2008.

[29] W. Dai, Q. Yang, G.-R. Xue, and Y. Yu, "Boosting for transfer learning," in *Proc. 24th Int. Conf. Mach. Learn.*, Corvalis, 2007, pp. 193–200.

[30] Y. Freund and R. E. Schapire, "A decision-theoretic generalization of on-line learning and an application to boosting," *J. Comput. Syst. Sci.*, vol. 55, no. 1, pp. 119–139, Aug. 1997.

[31] J. Jiang and C. Zhai, "Instance weighting for domain adaptation in NLP," in *Proc. 45th Annu. Meeting Assoc. Comput. Linguistics*, 2007, pp. 264–271.

[32] M. Chen, K. Q. Weinberger, and J. Blitzer, "Co-training for domain adaptation," in *Proc. 25th Annu. Conf. Neural Inf. Process. Syst.*, 2011, pp. 2456–2464.

[33] X. Kong, H. Gao, G. Shen, G. Duan, and S. K. Das, "FedVCP: A federated-learning-based cooperative positioning scheme for social Internet of Vehicles," *IEEE Trans. Comput. Soc. Syst.*, to be published, doi: 10.1109/TCSS.2021.3062053.

[34] Z. Gu *et al.*, "Epidemic risk assessment by a novel communication station based method," *IEEE Trans. Netw. Sci. Eng.*, vol. 9, no. 1, pp. 332–334, Jan. 2022.

[35] R. Pastor-Satorras, C. Castellano, P. Van Mieghem, and A. Vespignani, "Epidemic processes in complex networks," *Rev. Mod. Phys.*, vol. 87, no. 3, p. 925, 2015.

[36] M. Defferrard, X. Bresson, and P. Vandergheynst, "Convolutional neural networks on graphs with fast localized spectral filtering," in *Proc. Adv. Neural Inf. Process. Syst.*, Jun. 2016, pp. 3844–3852.

[37] T. N. Kipf and M. Welling, "Semi-supervised classification with graph convolutional networks," in *Proc. 6th Int. Conf. Learn. Representations*, 2017.

[38] S. Latif *et al.*, "Leveraging data science to combat COVID-19: A comprehensive review," *IEEE Trans. Artif. Intell.*, vol. 1, no. 1, pp. 85–103, Aug. 2020.

[39] S. Hochreiter and J. Schmidhuber, "Long short-term memory," *Neural Comput.*, vol. 9, no. 8, pp. 1735–1780, 1997.
[40] K. Cho, B. Van Merriënboer, D. Bahdanau, and Y. Bengio, "On the properties of neural machine translation: Encoder-decoder approaches," Sep. 2014. [Online]. Available: https://arxiv.org/abs/1409.1259
[41] L. Zhao *et al.*, "T-GCN: A temporal graph convolutional network for traffic prediction," *IEEE Trans. Intell. Transp. Syst.*, vol. 21, no. 9, pp. 3848–3858, Sep. 2020.

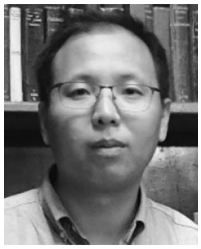

Xiangjie Kong (Senior Member, IEEE) received the B.Sc. and Ph.D. degrees from Zhejiang University, Hangzhou, China. He was an Associate Professor with the School of Software, Dalian University of Technology, Dalian, China. He is currently a Full Professor with the College of Computer Science and Technology, Zhejiang University of Technology, Hangzhou, China. He has authored or coauthored more than 130 scientific papers in international journals and conferences with more than 100 indexed by ISI SCIE. His research interests include network science, mobile computing, and computational social science. He is a Senior Member of the CCF and a Member of ACM.

Ning Li received the B.Sc. degree in computer science and technology in 2018 from the Zhejiang University of Technology, Hangzhou, China, where he is currently working toward the master's degree with the School of Computer Science and Technology. His research interests include machine learning, data science, and network science.

Chenwei Zhang received the Ph.D. degree in information science with the Ph.D. minor in computer science from Indiana University, Bloomington, IN, USA. She is currently an Assistant Professor with the Faculty of Education, University of Hong Kong, Hong Kong. Her research interests has two streams–one focuses on science of science, which studies the mechanisms underlying the doing of science and other stream mainly include data science, such as educational data mining, where a variety of computational approaches including machine learning and deep learning are applied for knowledge discovery.

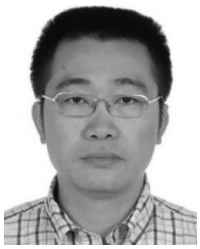

Guojiang Shen received the B.Sc. degree in control theory and control engineering and the Ph.D. degree in control science and engineering from Zhejiang University, Hangzhou, China, in 1999 and 2004, respectively. He is currently a Professor with the College of Computer Science and Technology, Zhejiang University of Technology, Hangzhou, China. His current research interests include artificial intelligence theory, Big Data analytics, and intelligent transportation systems.

Zhaolong Ning (Senior Member, IEEE) received the M.S. and Ph. D. degrees in communications and information system from Northeastern University, Shenyang, China, in 2011 and 2014, respectively. From 2013 to 2014, he was a Research Assistant with Kyushu University, Fukuoka, Japan. He is currently an Associate Professor with the School of Software, Dalian University of Technology, Dalian, China. He has authored or coauthored more than 120 scientific papers in international journals and conferences. His research interests include Internet of Things, mobile edge computing, deep learning, and resource management.

Tie Qiu (Senior Member, IEEE) received the Ph.D. degree in computer science from the Dalian University of Technology, Dalian, China, in 2012. He was an Assistant Professor with the School of Software in 2008 and an Associate Professor in 2013, Dalian University of Technology. From 2014 to 2015, he was a Visiting Professor with the Department of Electrical and Computer Engineering, Iowa State University, Ames, IA, USA. He is currently a Full Professor with the School of Computer Science and Technology, Tianjin University, Tianjin, China. He has authored or coauthored nine books, more than 150 scientific papers in international journals and conference proceedings, such as IEEE/ACM TRANSACTIONS ON NETWORKING, IEEE TRANSACTIONS ON MOBILE COMPUTING, IEEE TRANSACTIONS ON KNOWLEDGE AND DATA ENGINEERING, IEEE TRANSACTIONS ON INDUSTRIAL INFORMATICS, IEEE COMMUNICATIONS SURVEYS & TUTORIALS, IEEE COMMUNICATIONS, INFOCOM, and GLOBECOM. His 15 papers listed as ESI highly cited papers. He has contributed to the development of five copyrighted software systems and invented 16 patents. He is an Associate Editor for the IEEE TRANSACTIONS ON NETWORK SCIENCE AND ENGINEERING and IEEE TRANSACTIONS ON SYSTEMS, MAN, AND CYBERNETICS: SYSTEMS, an Area Editor of *Ad Hoc Networks (Elsevier)*, an Associate Editor for the *Computers and Electrical Engineering (Elsevier)*, *Human-centric Computing and Information Sciences (Springer)*, and a Guest Editor of *Future Generation Computer Systems*. He is also the General Chair, Program Chair, Workshop Chair, Publicity Chair, Publication Chair, and the TPC Member of numerous international conferences. He is a Senior Member of China Computer Federation and ACM.